

# Imaging structure with fluid fluxes at the Brady Geothermal Field, Nevada using satellite interferometric synthetic aperture radar (InSAR)

Gary Oppliger\*, U. of Nevada Reno, Mark Coolbaugh, U. of Nevada Reno

## Summary

We present an example of Interferometric Synthetic Aperture Radar's (InSAR) remarkable utility for defining an operating geothermal reservoir's lateral extent and hydrologically active fault systems. InSAR reveals millimeter-level surface deformation due to volume change in the reservoir and overlying aquifer systems caused by fluid pressure reduction and to a lesser extent temperature decrease. Fluid reinjection is revealed in the reverse process as surface inflation. The relevant characteristics and limitations of the InSAR method are discussed. We conclude that when integrated with other geophysical observations and reservoir production data, InSAR analysis will be able to guide new exploration and aid field management.

## Introduction

At the Brady geothermal field (Nevada, USA) poorly known reservoir boundaries add to the risk of new development and exploration work. Existing groundwater-level and pressure data are insufficient to delineate the geothermal field. In this context, InSAR mapped ground deformations provide valuable new information on the extent of the reservoir fracture system beyond the known field and on the effectiveness of reinjection wells.

Introduced only twelve years ago as a research method with the launch of the ERS 1 satellite, repeat-orbit differential InSAR has been showcased for its ability to image earth surface deformation related to earthquakes and volcanic intrusions and more recently ground deformation related to groundwater use, geothermal and petroleum production (Massonnet, 1998).

In a geothermal field, surface deformation occurs as a consequence of the production of geothermal fluids even if the reservoir is deep and isolated from shallow groundwater. Coupling into a shallow groundwater aquifer further enhances the deformation response. Reservoir deformation is largely driven by pressure reduction, which reduces the reservoir's compressive strength and allows subsidence of overlying strata into the reservoir. Contraction by cooling also contributes.

InSAR offers two distinct advantages over traditional optical leveling and GPS subsidence monitoring methods. First it can provide map-like images at resolutions of 20-40

meters covering 100 km by 100 km regions. Second, it can be applied in retrospective subsidence studies by using the 12 year archive of ERS 1/2 scenes.

InSAR's ability to monitor geothermal field subsidence has been established on some of the largest fields (Fialko, 2000) and models for inversion of reservoir volume strain have been developed and applied (Vasco, 2002). Here we examine the InSAR response over a mid-capacity geothermal field with the intent of demonstrating its effectiveness for revealing subsurface structure relevant to exploration.

## Interferogram Formation

With reference to the European Space Agency ERS 1/2 radar satellites and JPL's ROI PAC processing software, we outline the essential processing steps and data considerations.

### Radar Scene Acquisition and Focusing

The ERS 1/2 satellite illuminates the earth to the side of the satellite track with frequency modulated 5.3 GHz radar chirps repeated at 1.7 kHz. The ~4 km wide radar beam propagates across the terrain in the range direction returning a continuous "echo" stream to the satellite receiver. On the ground, chirp compression and Doppler filtering focus the raw radar return to an image with 20 m by 20 m ground resolution. Each ground resolution cell contains a single complex value representing the sum of the real (R) and imaginary (I) (i.e., in-phase and quadrature) returns from all reflectors in that cell. This focused radar image is referred to as Single Look Complex (SLC) image represented here as

$$SLC_1(x, y) = (R_1 + iI_1), \text{ where } i \text{ is } \sqrt{-1}.$$

### Interferogram Formation

SLC image pairs are spatially registered to better than 0.1 pixel using correlation algorithms; then the images are multiplied point-wise to produce the complex valued interferogram, INT:

$$INT(x, y) = (R_{12} + iI_{12}) = (R_1 + iI_1) (R_2 + iI_2)^*,$$

where  $*$  denotes the complex conjugate operator.

$$PHS(x, y) = \text{atan2}(I_{12}, R_{12}),$$

then defines the interferometric or phase difference between two images.

## Imaging structure with fluid fluxes

### Phase Fringes

In the special case of a zero baseline (or alternatively zero topography) and no ground deformation, the interferogram phase is theoretically constant across the scene. Local ground deformation in the interferogram period alters the radar travel distance and is expressed as a relative phase anomaly over the deformed area. In the general case of a non-zero baseline with topography, a terrain related phase pattern occurs that is easily predicted and removed using a digital elevation model. Where ground deformation exceeds half the radar wavelength, (2.83 cm) the phase vector wraps around, constraining phase between 0 to  $2\pi$ . These  $2\pi$  intervals are referred to as phase fringes and are colored in the figures with one full cycle of the color pallet. The average  $23^\circ$  radar incidence angle of the ERS 1/2 satellite renders it 2.4 times as sensitive to vertical displacement as to displacement in the best coupled horizontal component. One fringe is produced by either 3.07 cm of vertical or 7.24 cm of orbit-track-perpendicular horizontal ground displacement.

### **Interferogram Signal and Noise**

#### Selecting SLC Image Pairs

Baseline and time separation are primary interferogram parameters. Preferred scene pairs have no more than 300 meters offset (or perpendicular baseline) in their orbital paths perpendicular to the radar line-of-sight (LOS) vector. The time separation between scenes must be long enough to allow the surface deformation patterns to be well expressed in the interferogram, but not so long that heavy vegetation growth or other surface processes cause a loss of phase correlation between the images.

#### Decorrelation Signal Dropouts

In many regions vegetation growth drives decorrelation and sets the maximum effective interferogram time interval. In our study area in the Great Basin, sage and scrub growth over five years has little effect. However, we find that areas with wind blown sand or playas are subject to relatively rapid decorrelation.

#### Dynamic Range

InSAR's deformation observation dynamic range is subject to time and spatial constraints. On the minimum signal side, our experience has shown under good atmospheric and ground conditions, surface deformation features with 100 m to 5 km widths and 5 mm displacement over five years can be reliably imaged in a single interferogram. Under these favorable conditions, the non-deformation in-band noise is about 1 - 2 mm. Use of multiple interferograms can further reduce this noise level. On the maximum signal side, there is no practical limit on the total observable deformation, as long as the horizontal gradient

in surface displacement projected on the radar LOS vector does not exceed one-half wavelength per ground resolution cell (20 meters) during the interferogram interval.

Our experience suggests for geothermal field observations, a range of interferogram time intervals is desirable to observe both long-wavelength, low-amplitude features distal to the field and short-wavelength, high-amplitude detail near production centers.

#### Noise

Tropospheric water vapor variation is the dominate source of in-band noise and occasionally mimics a few centimeters of surface deformation. It is identified and avoided by the use of multiple interferogram periods. Short wavelength out-of-band decorrelation noise can be reduced by spatial filtering at the expense of detail.

### **Interpretation of Structure from the Deformation Field**

#### The Brady Geothermal Field

The Brady geothermal field lies along the northwest structural boundary between the low relief Hot Springs Mountains and Hot Springs Flats basin, about 80 km east-northeast of Reno, Nevada (Benoit, 1982, Faulds, 2003). The fault-controlled reservoir is developed in Mesozoic metamorphic basement rocks and is overlain by 800 meters or more of Tertiary volcanic and sedimentary rocks. Mesozoic basement structure and relief is suggested by surface gravity data (Figure 1). The Brady 21-MW dual-flash geothermal plant produces from three clusters of production wells (distributed over ~1.4 km) with an average depth of 930 meters and average fluid temperature of ~156 C. The plant has three clusters of injection wells (spaced over 7 km) with an average injection fluid temperature of ~114 C.

Our interferograms (Figures 2 and 3) reveal the first subsidence feature reported for the Brady geothermal field. The interferograms show the production zone has an inner strong hydrologic conductivity zone along a 7 km axis with an outer weaker but identifiable depression zone for 11 km total. This is about 6 km more strike length than was previous known.

Maximum subsidence in the production area is at least 1.3 cm/year. Along northwest profiles, subsidence is centered on the NNE trending Brady fault system and has a bell-form with a ~1.2 km half-width and well defined asymptotes over 4 km on either side.

Over the two interferogram periods A and B (Figures 2, 3) the subsidence pattern grows asymmetrically toward the south-southeast, probably reflecting evolving reservoir fluid drawdown. Partitioning of the subsidence is not

## Imaging structure with fluid fluxes

apparent during the first period but becomes evident during the second period with the appearance of two elliptical lobes that are separated by an injection well. An unexpected bifurcation exists in the subsidence axis north of the known reservoir. One trend continues on a NNE strike, the other trends to the NE. These are further discussed below.

Changing production and reinjection patterns may illuminate distinct hydrologic structures. In Interferogram B (Figures 3 and 4), a strong asymmetric inflation feature, 1 km wide and 3 km long, appears just northeast of the northern cluster of injection wells. This injection feature is confined to the structural zone delineated by the drawdown pattern in the previous interferogram interval. The southern boundary of the inflation feature terminates abruptly within the main deflation feature, 300 meters north of the injection well. This asymmetry is consistent with very rapid return of the cooled injectate into the production zone - a situation observed in production during this period.

To solve this problem the operators added a reinjection well cluster south of the known field in late 1999. This well cluster is outside the reservoir's InSAR indicated extended hydrologic zone, so it may ultimately be ineffective at recharging the reservoir. Additional interferograms covering the period after 2000 will help assess this.

### Subsidence sensitivity to fluid flux

Over the study period, annual extraction has averaged 17 million kg (M kg). Recharge through injection wells averaged 81 percent and at least 4 percent through percolation ponds. Hence we estimate the average annual mass deficit at about 3M kg. Volumetrically, approximately half of the InSAR subsidence is concentrated in a 1.2 km by 4.2 km (5 square km area) where it averages 0.5 cm per year. Therefore, associating half of the 3M kg fluid volume loss with that area, the average vertical fluid flux per square meter in the production area is 30 cm (or 3 meters of equivalent water table drop at 10% porosity). The subsidence to fluid flux sensitivity is, thus, estimated as  $0.5 \text{ cm} / 30 \text{ cm} = 0.017$ . We can conclude for this area that water table changes of as little as 3 meters will produce robust InSAR subsidence signals. Further, trends in annual water table changes of 0.5 meters per year will become well resolved over a 6-year time span.

### **Conclusions**

InSAR is just beginning to reveal its potential to trace and characterize the hydrologically active fracture and fault systems in geothermal reservoirs. When integrated and validated with other geophysical observation and reservoir production information, such analysis can guide new

exploration wells and improve field management by improving reinjection patterns. We note that the cost of a multiple interferogram InSAR geothermal field study is comparable to an aeromagnetic or ground gravity survey.

### **References**

- Benoit, W.R., Hiner, J.E., and Forest, R.T., 1982, Discovery and geology of the Desert Peak geothermal field: A case history: Nevada Bureau of Mines and Geology Bulletin 97, 82 p.
- Faulds, J., Garside, L., Oppliger, G., 2003, Structural Analysis of the Desert Peak-Brady Geothermal Fields, Northwestern Nevada, Geothermal Resources Council Transactions Vol. 27.
- Fialko, Y., and M. Simons, 2000, Deformation and seismicity in the Coso geothermal area, Inyo County, California: Observations and modeling using satellite radar interferometry, *J. Geophys. Res.*, 105, 21,781-21,794.
- Massonnet, D. and Feigl, K. L., 1998, Radar interferometry and its application to changes in the earth's surface, *Reviews of Geophysics*, 36(4);441-500.
- Vasco, D.W., C. Wicks, and K. Karasaki, 2002, Geodetic imaging: High-resolution reservoir monitoring using satellite interferometry, *Geophys. J. Int.*, 149, 555-571.

### **Acknowledgements**

This work was supported by the Department of Energy under DE-FG36-02ID14311 through the Great Basin Center for Geothermal Energy. Additional support was provided by the Arthur Brant Laboratory for Exploration Geophysics, University of Nevada Reno.

The European Space Agency ERS 1/2 raw SAR scenes were provided through the Western North American InSAR (WInSAR) research consortium.

JPL's ROI\_PAC Research Interferometry package was used to prepare the interferograms.

Ormat International Inc. assisted by providing raw geothermal production records for the Brady field, but the authors take responsible for any errors in its application.

## Imaging structure with fluid fluxes

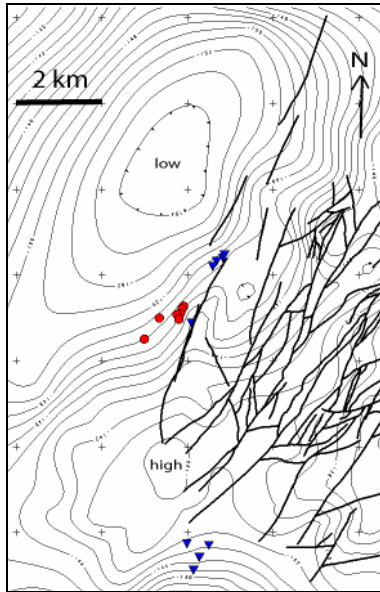


Figure 1: CBA gravity with 1 milligal contours reflects structure and depth to Mesozoic basement. Production wells: circles (red). Injection wells: triangles (blue). Surface faults: heavy black lines.

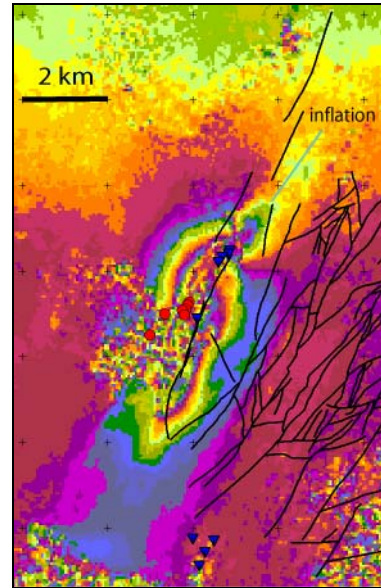


Figure 3: Interferogram B - 4.78 years: 95-11-04 to 00-09-24. Each color represents 0.16 cm line-of-sight LOS distance change. A full fringe color cycle is 2.83 cm LOS or 3.07 cm vertical. Surface faults: heavy black lines

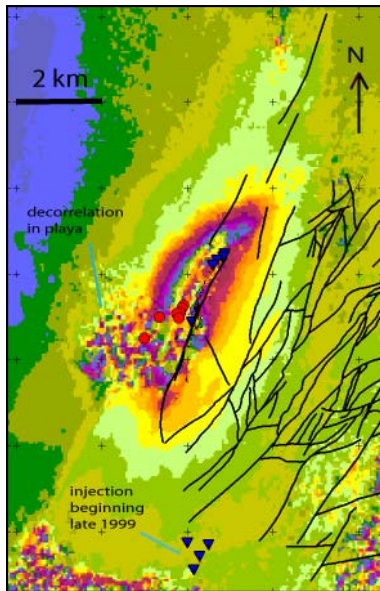


Figure 2: Interferogram A - 2.96 years: 92-11-26 to 95-11-04.

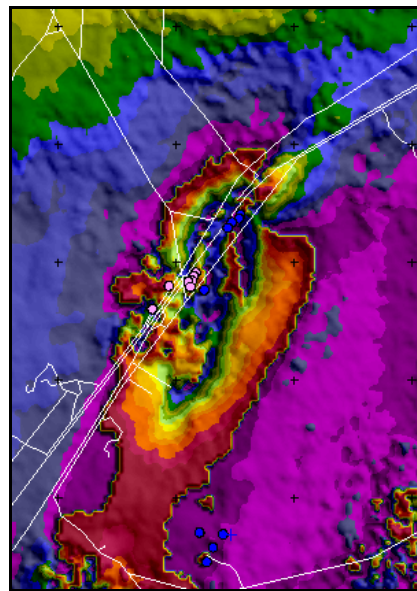


Figure 4: Shaded-relief of filtered Interferogram B (Figure 3). Shading aids recognition of inflation. Roads: white lines.